

PAPER

Adsorption of Ag, Au, Cu, and Ni on MoS₂: theory and experiment

To cite this article: Haley Harms et al 2025 J. Phys.: Condens. Matter 37 015001

View the article online for updates and enhancements.

You may also like

- He-lon Induced Defect Generation and Doping of 2D MoS2 Monolayers
 Frederick Aryeetey, Dilbagh Singh, Kyle Nowlin et al.
- Effect of annealing temperature on the microstructure and optical properties of MoS₂ films

Bianlian Zhang, Zhen Cheng and Yu Meng

- Engineering Stepped Edge Surface Structures of MoS2 Sheet Stacks to Accelerate the Hydrogen Evolution Reaction

Jue Hu, Bolong Huang, Chengxu Zhang et

J. Phys.: Condens. Matter 37 (2025) 015001 (7pp)

https://doi.org/10.1088/1361-648X/ad7fae

Adsorption of Ag, Au, Cu, and Ni on MoS₂: theory and experiment

Haley Harms¹, Andrew J Stollenwerk¹, Connor Cunningham¹, Caden Sadler¹, Evan O'Leary², Timothy E Kidd¹ and Pavel V Lukashev^{1,*}

E-mail: pavel.lukashev@uni.edu

Received 11 June 2024, revised 2 August 2024 Accepted for publication 25 September 2024 Published 14 October 2024



Abstract

Here, we present results of a computational and experimental study of adsorption of various metals on MoS₂. In particular, we analyzed the binding mechanism of four metallic elements (Ag, Au, Cu, Ni) on MoS₂. Among these elements, Ni exhibits the strongest binding and lowest mobility on the surface of MoS₂. On the other hand, Au and Ag bond very weakly to the surface and have very high mobilities. Our calculations for Cu show that its bonding and surface mobility are between these two groups. Experimentally, Ni films exhibit a composition characterized by randomly oriented nanoscale clusters. This is consistent with the larger cohesive energy of Ni atoms as compared with their binding energy with MoS₂, which is expected to result in 3D clusters. In contrast, Au and Ag tend to form atomically flat plateaued structures on MoS₂, which is contrary to their larger cohesive energy as compared to their weak binding with MoS₂. Cu displays a surface morphology somewhat similar to Ni, featuring larger nanoscale clusters. However, unlike Ni, in many cases Cu exhibits small plateaued surfaces on these clusters. This suggests that Cu likely has two competing mechanisms that cause it to span the behaviors seen in the Ni and Au/Ag film morphologies. These results indicate that calculations of the initial binding conditions could be useful for predicting film morphologies. In addition, out calculations show that the adsorption of adatoms with odd electron number like Ag, Au, and Cu results in 100% spin-polarization and integer magnetic moment of the system. Adsorption of Ni adatoms, with even electron number, does not induce a magnetic transition.

Keywords: transition metal dichalcogenides, surface morphology, binding energy

1. Introduction

Research on two-dimensional layered materials has been a driving force in condensed matter physics for some time. One class of materials, the transition metal dichalcogenides (TMDC) have attracted particular attention due in large part to high tunability of their properties, e.g. by mechanical strain [1–4], atomic intercalation and defects [5–8], chemical adsorption

[9, 10], etc. Molybdenum disulfide, as a naturally available and inert semiconductor, is one of the most studied TMDCs, with many practical applications, such as hydrogen storage [11], tribology [12], photovoltaic and catalytic applications [13, 14], batteries [15], transistors [16], defect engineering [17], etc.

An important consideration for 2D compounds is how they interact with other materials, especially at their interface with metals. The van der Waals (vdW) terminated surfaces can create interesting film growth behaviors that are critical for understanding the potential device integration. Owing to their weak bonding and large lattice mismatch with most metals, it

¹ Department of Physics, University of Northern Iowa, Cedar Falls, IA 50614, United States of America

² Department of Physics and Astronomy, Iowa State University, Ames, IA 50011, United States of America

^{*} Author to whom any correspondence should be addressed.

is appropriate to examine the adsorption of various elements on their surface [18–20]. In particular, adsorption induced magnetic properties and metallic behavior has been reported in graphene [21, 22] and MoS₂ [9, 23, 24]. These and similar reports indicate that the physical properties of vdW materials are very sensitive to adsorption, e.g. one can control the band gap and other properties of semiconducting TMDCs, which may have practical applications in optoelectronics and various tunnel junction based devices.

In the current work, we present a computational and experimental study of adsorption of four metallic elements (Au, Ag, Cu, Ni) on the surface of MoS₂. We find that the initial binding characteristics of these adsorbed elements can sometimes be correlated with their film growth morphology. As expected, a combination of strong binding and large lattice mismatch leads to nanocluster formation as seen in the Ni/MoS2 system. Interestingly, we have found that weak bonding and high mobility result in atomically flat terraces to be formed [25, 26]. While there are some differences, Au and Ag show similar growth morphologies in this regime. While all the metals showed nanocluster formation for very low coverage, the Au and Ag films coalesce with large lateral areas intact despite lattice mismatch of over 8%. Cu growth characteristics are in between those seen in Ni and Au/Ag suggesting more than one competing mechanism that cause it to span the characteristic of these two sets of

The rest of this paper is organized as follows. In Section II, we outline the computational and experimental techniques employed in this work. The main results are presented in Section III, which consists of computational and experimental sub-sections. The concluding remarks are presented in Section IV, which is followed by acknowledgments to the funding sources and external facilities. The references to the relevant literature are presented at the end of the paper.

2. Methods

2.1. Computational methods

All calculations used in this work are performed with the Vienna *ab initio* simulation package [27], within the projector augmented-wave method [28] and generalized-gradient approximation [29]. This method has been reported in literature to adequately treat the adsorption of various adatoms on MoS_2 [9, 24]. The integration method by Methfessel and Paxton [30] is used, with a cut-off energy set to 500 eV. The Brillouin-zone integration is performed with the *k*-point mesh of $4 \times 4 \times 1$ for structural optimization, and $8 \times 8 \times 1$ for the self-consistent calculations. The energy convergence criterion is set to 10^{-3} meV for the total energy calculations, and to 10^{-2} meV for the atomic relations. We did not include vdW correction in our calculations, At the same time, we performed some test calculations, which confirmed that inclusion of this correction does not affect our main results (binding energy and

electronic structure). In particular, we calculated the binding energy and density of states of Ag/MoS₂ with and without the vdW correction (method of Grimme with zero-damping function), and the results essentially did not differ. Some of the input files are set up with the MedeA® software environment, which is also used for visualizing the crystal structures [31]. All calculations are performed using the Advanced Cyberinfrastructure Coordination Ecosystem: Services & Support (formerly known as Extreme Science and Engineering Discovery Environment) resources located at the Pittsburgh Supercomputing Center [32], and with the resources of the Center for Functional Nanomaterials at Brookhaven National Laboratory.

The adsorption of metallic adatoms on the surface of MoS_2 is simulated as follows. First, we constructed a $4\times4\times1$ supercell of a monolayer of MoS_2 (16 Mo atom, 32 S atoms), with a vacuum layer of 20 Å imposed in the vertical direction. The latter is used to avoid the potential overlap of wavefunctions in the direction of stacking. Then, we relaxed the geometry (volume and atomic positions) of this cell. Subsequently, we placed a single atom of a metal at one of the seven sites, as discussed below in the text. The vertical distance of the metallic atom from the surface of MoS_2 was then relaxed. The in-plane positions of the adatoms were fixed during optimization. Figure 1 illustrated the geometry of the considered cell (see discussion below for more details).

2.2. Experimental methods

Au, Cu, Ag, and Ni samples were each prepared via room temperature depositions onto mechanically cleaved MoS₂ (SPI Supplies) as reported previously [25, 26, 33, 34]. Experimental results are carried out on bulk MoS₂. To prepare the Au sample, the freshly cleaved MoS2 was placed in a vacuum deposition chamber (base pressure 2×10^{-9} mbar). Deposition of Au was achieved through thermal evaporation of Au pieces (99.999% pure) in a BN basket. The Au samples were then transferred from the deposition chamber to the STM scanning chamber for analysis. Depositions for Cu, Ag, and Ni were carried out in situ using a mini electron-beam evaporator (MANTIS QUAD-EV) within a vacuum chamber (base pressure 5×10^{-10} mbar). Deposition occurred using Cu pieces (99.999% pure) in a molybdenum crucible fitted with an alumina liner, a 2 mm Ag wire (99.999% pure), and a 2 mm Ni wire (99.995% pure). Consistent deposition rates on the order of 0.1 Å s^{-1} were obtained using either a flux monitor or were calculated from the resulting scanning tunneling microscopy images. All materials were deposited with a nominal thickness ranging from approximately 8 nm to 12 nm $\pm 10\%$. Prepared samples were then transferred to a variable temperature STM system scanner head (Omicron). STM tips were mechanically cut from a 0.25 mm Pt₉₀Ir₁₀ wire. The scanning parameters used in this study were kept relatively consistent with the tunneling bias and current set point at approximately 1 V and 1 nA, respectively.

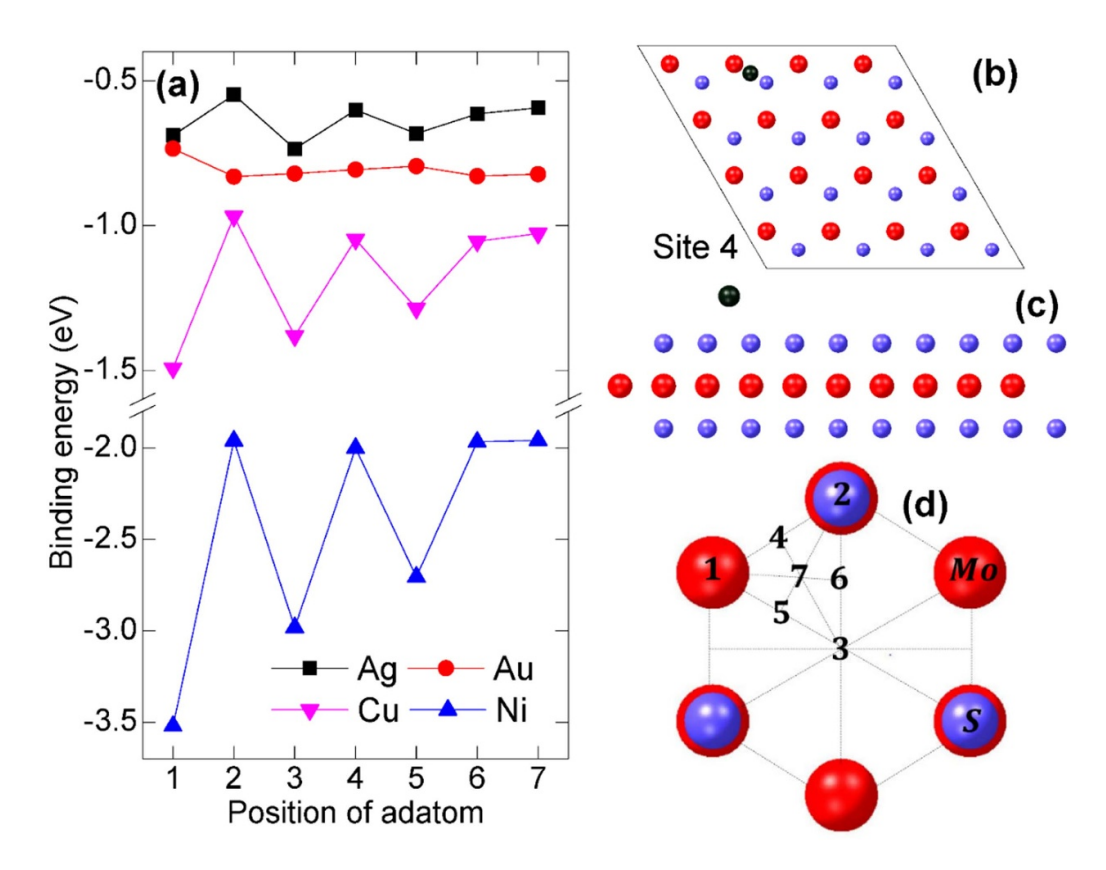


Figure 1. (a) Calculated binding energies of Ag (black line and squares), Au (red line and circles), Cu (magenta line and down facing triangles), and Ni (blue line and up facing triangles) adatoms on the surface of MoS₂. (b) and (c) Crystal structure of the considered cells (top and side views, correspondingly). (d) Seven considered positions/sites of adatoms on MoS₂. As an example, site 4 is shown in figures (b) and (c).

3. Results and discussion

3.1. Computational results

3.1.1. Binding of adatoms with MoS₂ surface. Figure 1(a) shows calculated binding energies of 4 different adatoms (Ag, Au, Cu, and Ni) on the surface of a MoS₂ monolayer. The binding energies of each adatom are colored/labeled as indicated in the figure. The crystal structure used in our calculations is shown in figures 1(b) (top view) and (c) (side view). We considered 7 possible adsorption sites, which are shown in figure 1(d) (as an example, site 4 is shown in figures 1(b) and (c)). This allowed us to determine the lowest energy adsorption location, as well as qualitatively estimate the mobility of the adsorbed element, as will be discussed below. The binding energies shown in figure 1(a) are calculated as follows.

$$E_{\text{binding}} = E_{\text{MoS}_2 + \text{adatom}} - E_{\text{MoS}_2} - E_{\text{adatom}}.$$

Here, $E_{\rm binding}$ is the calculated binding energy, $E_{\rm MoS_2+adatom}$ is the calculated energy of a MoS₂ monolayer with adsorbed adatom, $E_{\rm MoS_2}$ is the calculated energy of MoS₂ monolayer, and $E_{\rm adatom}$ is the calculated energy of a single atom of the adsorbed element. The latter was estimated by placing a single atom in a $15\text{\AA} \times 15\text{\AA} \times 15\text{Å}$ 'box' and calculating its energy.

As seen in figure 1(a), the strongest binding to the MoS_2 monolayer of the four considered elements is exhibited by Ni.

In addition, our calculations indicate that site 1 (i.e. adatom is placed above Mo) is energetically preferred by Ni. Moreover, the next energetically preferred position is site 3 (adatom placed in the hollow site at the center of the hexagon, see figure 1(c)), but the calculated energy difference between these two sites is very large (around 0.5 eV). Even the interstitial site between these two potential bonding locations has a binding energy of around 300 meV, indicating that Ni adatoms should have low mobility even if the films were annealed to several hundred Kelvin.

Of the four considered elements, the weakest binding to the MoS₂ monolayer is exhibited by Ag, closely followed by Au. Both of these elements exhibit very high mobility, with the energy difference between preferred and interstitial sites less than 100 meV. Au is especially interesting as it has a different preferred site atop a S atom and the energy difference between this and all other sites, except the site directly above Mo, is on the order of k_BT at room temperature (figure 1(a)). There are a large number of sites for the Au and Ag adatoms on the MoS₂ surface that are approximately one kT of the lowest energy site. Given the high energy of these adatoms during the deposition process, it is probable that additional Au and Ag will not always position themselves in the lowest energy location associated with a single adatom. It is more likely that additional adatoms could move to other sites that would lower the overall energy associated with thicker films, thereby relieving

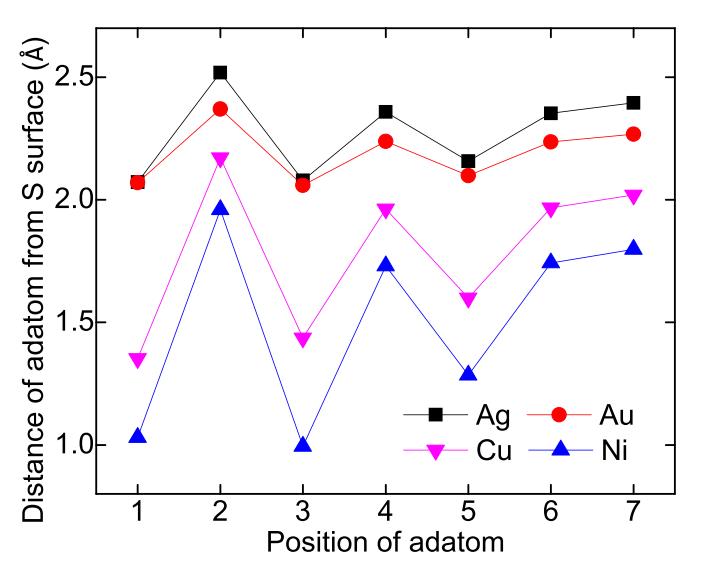


Figure 2. Calculated equilibrium distances of Ag (black line and squares), Au (red line and circles), Cu (magenta line and down facing triangles), and Ni (blue line and up facing triangles) adatoms from the surface of MoS_2 monolayer, i.e. the perpendicular distance of adatoms from the S-layer.

strain at the interface. This strain alleviation is likely one of the key mechanisms that enables the films to exhibit electronic growth modes [25, 26], which are especially strong in Au [35].

The binding energy and mobility of Cu would seem to be in between that of Ni and the other noble metals. This is reflected in our recent determination that Cu exhibits both the preferred heights seen in Au and Ag, but also demonstrates cluster formation as seen in Ni [34]. It is interesting that Ag, Cu, and Ni all have very similar site binding energy profiles, with the only significant difference being one of scale. Each of these three elements has a significant preference for sites 1, 3, and 5 which limits both mobility and how interface strain can be alleviated, although the overall bonding energy is so weak for Ag this is less of an issue. The weak bonding and nearly flat site binding energy profile for Au seems quite unusual, and is likely why even gold nanoparticles have been found to be mobile on the MoS₂ surface [25].

Figure 2 shows calculated equilibrium distances of Ag, Au, Cu, and Ni adatoms from the surface (i.e. S-layer) of the MoS₂ monolayer (adsorbed elements are colored/labeled as indicated in the figure). As one can see from the figure, the smallest equilibrium distance from the surface of MoS₂ is exhibited by Ni (around 1 Å), followed by Cu, then Au/Ag (the latter two elements are more or less equidistant from MoS₂). These results are consistent with the calculated binding energies. In particular, the strongest binding of Ni adatom with the MoS₂ surface results in the smallest distance between them. On the opposite end, Ag/Au exhibit the weakest bonding with the MoS₂ surface, and as a result the distance between them is comparatively large (twice larger than for the case of Ni). Both the binding energy and the distance from the MoS₂ surface of Cu have intermediate values, between Ni and Ag/Au.

3.1.2. Electronic and magnetic structure. Figure 3(A) shows calculated total density of states (DOS) of a MoS2 monolayer with the 4 considered adatoms. The density of states of a pure MoS₂ monolayer (without adatom) is also shown for comparison, and it is consistent with the results reported in literature [36]. As seen from figure 3(A), of the four considered adsorbed adatoms, Ni exhibits a distinctly different behavior compared with Ag, Au, and Cu. In particular, adsorption of Ni adatom on the MoS₂ surface retains the semiconducting nonspin-polarized non-magnetic nature of the system. Essentially, adding Ni adatom to the surface of MoS2 does not result in any significant changes of electronic and magnetic properties of the system (compare figures 3(a) and (e)), except for emergence of Ni states close to the Fermi level, as discussed below. At the same time, adding Ag, Au, and Cu adatoms on a MoS₂ surface results in a transition to 100% spin-polarized state, with an integer value of magnetization (1.000 μ_B /cell). The difference in the behavior of Ni compared with Ag, Au, and Cu is due to the number of electrons in these elements. In particular, Ag, Au, and Cu are group 11 elements and thus contain one unpaired electron, which results in an integer magnetic moment of a single atom. At the same time, Ni is a group 10 element with an even number of electrons, thus a single Ni atom has zero magnetic moment. In addition, when Ag, Au, and Cu adatoms are placed on the surface of MoS2, this results in a hybridization of their states with their nearest neighbor Mo and S atoms, which also exhibit magnetic behavior. This is illustrated in figures 3(B) and (C) for the case of Cu and Ni respectively (Au and Ag exhibit behavior similar to Cu).

Figures 3(B) and (C) show element resolved density of states for Cu/MoS₂ and Ni/MoS₂, respectively (the electronic structures of Ag/MoS2 and Au/MoS2 are similar to that of Cu/MoS₂ and are not shown here for brevity). As seen from figure 3(B), Cu, Mo, and S have comparable contributions to the large spin-polarization/magnetic moment. More specifically, the largest contribution to the integer magnetic moment comes from the Mo atom, which is the nearest neighbor of the Cu adatom. The next nearest neighbor Mo and S atoms also have sizable contributions to the magnetization, but starting from the second nearest neighbors, the magnetic moments of Mo and S atoms become more or less negligible. At the same time, as seen in figure 3(C), adsorption of Ni adatom at the surface of MoS₂ produced Ni states right below the Fermi level. Due to hybridization with nearest neighbor Mo and S atoms, these elements also contribute to the states at the Fermi level. Yet, these states are essentially non-spin-polarized, thus the system is non-magnetic. In addition, Ni/MoS2 also retains its semiconducting properties, with a band gap just barely smaller than that in a pristine MoS₂ monolayer.

3.2. Experimental results

Figure 4 shows 200 nm by 200 nm STM images of \sim 10 nm films of Au (4 a), Ag (4 b), Cu (4 c), and Ni (4 d) deposited at room temperature with no annealing. The gold film is very homogenous and nearly atomically flat with surface variation no more than \pm 2 atomic layers. The Ag film also results

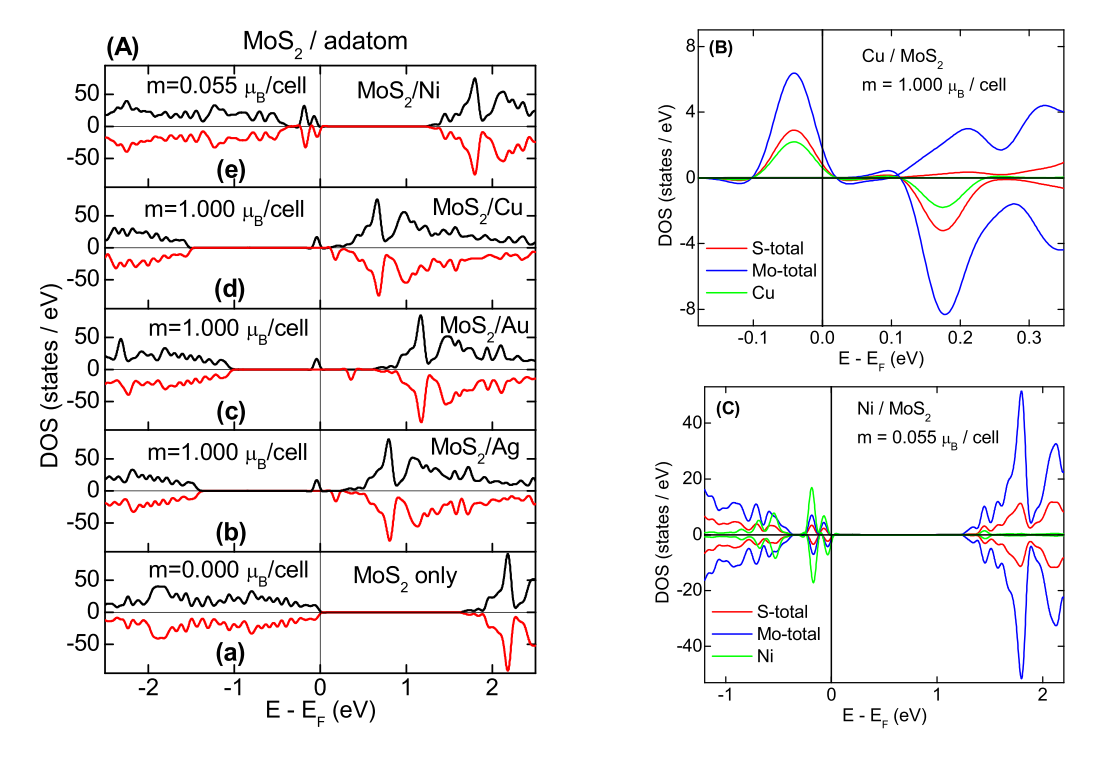


Figure 3. (A) Calculated total density of states of MoS₂ monolayer (a), MoS₂/Ag adatom (b), MoS₂/Au adatom (c), MoS₂/Cu adatom (d), MoS₂/Ni adatom (e). Black line/positive DOS correspond to spin-up states, red line/negative DOS correspond to spin-down states. Solid vertical line indicated position of the Fermi level. Calculated total magnetic moments per cell are shown in the figure. (B) and (C) Calculated element resolved DOS of Cu/MoS₂ and Ni/MoS₂, correspondingly.

in atomically flat, with \pm 1 atomic layers, curved plateaus with relatively large lateral dimensions. However, the curved plateaus are separated by deep trenches reaching down to the MoS₂ surface in some locations. Unlike Au and Ag, Cu forms a mixture of plateaued and rounded clusters with diameters on the order of 5 nm and Ni forms rounded structures with a diameter of 2 nm.

The difference in binding energy for different sites, including interstitials, is a good indication of the mobility of adatoms on the MoS₂ surface. In particular, it can play a decisive role in relieving the mechanical strain at the interface caused by the lattice mismatch. Strain is normally determined by a combination of the bonding strength and lattice mismatch, which is quite large for all atoms, over 8% for Ag, Au, and Cu and over 20% for Ni. High mobility enables the metal atoms to better reach equilibrium at lower temperatures, and strain relief enables films to grow laterally with less disruption. Hence the higher strain expected for Ni and Cu should result in nanometer scale clusters as seen in the experimental data. As discussed previously, the Cu exhibits intermediate behavior in having both cluster formation like Ni as well as plateaued surfaces like Au or Ag, albeit on a smaller scale. The larger lateral size for the Cu clusters is also indicative of the smaller strain expected to be felt at the Cu/MoS₂ interface as compared to Ni/MoS₂.

Another important consideration for the observed surface morphology is the relative bonding strength between the metals themselves (i.e. their cohesive energies) and their bonding to MoS₂. For example, one can compare the binding

energies of different metals on MoS₂ with their metal cohesion energies. This data is shown in table 1 and includes the calculated binding energies (E_{bnd}) for all seven considered adsorption sites of the considered 4 elements. Also included in this table are the absolute values of the metal cohesive energies (E_{coh}) taken from [37]. As seen in table 1, the cohesive energy of Au and Ag is significantly larger than the binding energy of these elements on MoS₂. Under the assumption that this is the only physical mechanism that determines the growth of these elements on MoS₂, they should all follow a 3D nucleation growth pattern rather than the layer-by-layer growth seen with Au and Ag. The formation of atomically flat structures may be due to a preference of these elements to bond to the edge of the cluster rather than on its top. One possible explanation of this is a high preference of these elements to bind with sulfur (adsorption site 3 (see figure 1)) as well as with itself. Once a seed layer is formed, one would expect a layer-by-layer growth to proceed. As shown in figures 4(c) and (d), Cu and Ni form small 3D nanoclusters as expected based on the comparison between the binding energy to MoS₂ and their respective cohesive energies. Ni cluster formation is also exacerbated by a high interfacial stress caused by a low mobility and large lattice mismatch (\sim 21%) with MoS₂. Cu has a mobility that lies in between Ni and Au/Ag. This would help relieve the strain at the interface but would not explain the occurrence the plateaued clusters observed experimentally. We speculate that surface morphology of Cu is due to a competition between the tendency of additional Cu adatoms to bond with themselves (thus forming 3D clusters) and the need to bond to the edge of

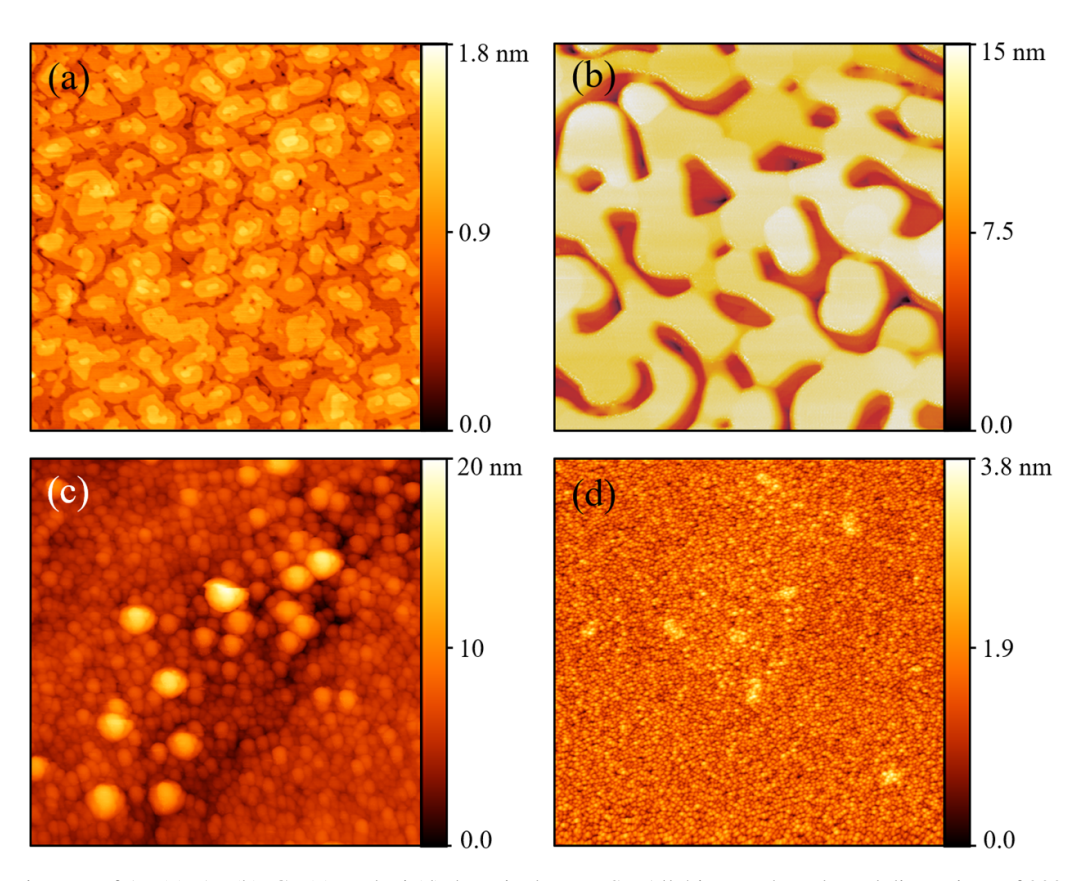


Figure 4. STM images of Au (a), Ag (b), Cu (c), and Ni (d) deposited on MoS₂. All 4 images have lateral dimensions of 200 nm by 200 nm.

Table 1. Calculated binding energies (E_{bnd}) for all seven considered adsorption sites of the considered 4 elements; as well as metal cohesive energies (E_{coh}) taken from [37]. The energies are in eV.

	Site 1	Site 2	Site 3	Site 4	Site 5	Site 6	Site 7	E _{coh}
Au	-0.73438	-0.83059	$-0.820\ 54$	-0.80682	-0.79487	$-0.829\ 18$	$-0.822\ 60$	3.81
Ag	-0.68871	-0.54842	$-0.735\ 15$	-0.60093	-0.68191	-0.61431	-0.59289	2.85
Cu	-1.49289	$-0.968\ 56$	-1.38185	-1.04762	-1.28645	-1.05482	-1.02750	3.49
Ni	-3.52047	-1.96051	$-2.981\ 68$	$-2.001\ 06$	$-2.705\ 58$	-1.96688	$-1.958\ 68$	4.44

the cluster to form plateaued structures like Au and Ag. Further studies are needed to get better understanding of the role of edge bonding to the observed surface morphology.

4. Conclusions

In this work, we presented results of a computational and experimental study of adsorption of four different metals on MoS₂. In particular, we analyzed the binding mechanisms of four metallic elements (Au, Ag, Cu, Ni) on MoS₂. Among these elements, Ni exhibits the strongest binding/lowest mobility on the surface of MoS₂. The weakest binding is exhibited by Ag, closely followed by Au which also exhibits the highest mobility. Cu exhibits somewhat intermediate values of both the binding energy and mobility on the surface of MoS₂. If we only examine the binding energy of these elements with MoS₂ to their respective cohesion energies, we expect all four elements to undergo 3D growth. Experimentally, this is clearly not the case for Au and Ag

on MoS₂, which exhibit large plateaued structures. Among other things, this may be due to the fact that these elements prefer to bond to the edge of a cluster rather than the top, resulting in the 2D plateau structures we observe. The relatively large size of the plateaued structure is likely due to the high mobility of these two elements, which allow these elements to reach their lowest energy state and relieve strain at the interface. Ni appears to be the only element that exhibits prototypical 3D growth expected for an element with a cohesive energy much larger than its binding energy with the substrate. Experimentally, Cu shows characteristics of cluster formation as well as plateaued surfaces. The cluster formation is likely due to the strong cohesive energy as well as the reduced mobility relative to Au and Ag. The plateaued surfaces are likely due to a strong tendency for Cu to bind to the edge of a cluster. These two mechanisms appear to be in competition and would explain why Cu exhibits characteristic of both the Ni and Au/Ag films. In addition to surface morphology study, our calculations indicate the odd electron bearing metals induce a half metallic magnetic transition in the MoS₂ monolayer and the even electron bearing Ni does not. This may have applications in forming magnetic nanoclusters as seen with Au [38].

Data availability statement

The data that support the findings of this study are available at the following website: https://doi.org/10.7910/DVN/PEN1ZG

Acknowledgment

P V L was supported by the National Science Foundation (NSF) (Expanding Capacity in Quantum Information Science and Engineering (ExpandQISE)) under Grant Number 2328889. A J S and T E K were in part supported by the US Department of Energy (DOE) under Award Number DE-SC0020334. H A H and C C were supported in part by the National Science Foundation (Grant Nos. DMR-2300639). This work used the Advanced Cyberinfrastructure Coordination Ecosystem: Services & Support (ACCESS) (formerly known as Extreme Science and Engineering Discovery Environment (XSEDE)), which is supported by National Science Foundation Grant Numbers ACI-1548562. This work used the ACCESS Regular Memory (Bridges 2) and Storage (Bridges 2 Ocean) at the Pittsburgh Supercomputing Center (PSC) through allocation TGDMR180059, and the resources of the Center for Functional Nanomaterials, which is a U.S. DOE Office of Science Facility, and the Scientific Data and Computing Center, a component of the Computational Science Initiative, at Brookhaven National Laboratory (BNL) under Contract No. DE-SC0012704.

ORCID iDs

Andrew J Stollenwerk https://orcid.org/0000-0001-7083-

Connor Cunningham https://orcid.org/0009-0008-3222-7791

Caden Sadler https://orcid.org/0009-0003-6853-3276 Pavel V Lukashev https://orcid.org/0000-0002-2551-5954

References

- [1] Scalise E, Houssa M, Pourtois G, Afanas'ev V and Stesmans A 2012 *Nano Res.* **5** 43
- [2] Lu P, Wu X, Guo W and Zeng X 2012 Phys. Chem. Chem. Phys. 14 13035
- [3] Yue Q, Kang J, Shao Z, Zhang X, Chang S, Wang G, Qin S and Li J 2012 Phys. Lett. A 376 1166
- [4] Tabatabaei S, Noei M, Khaliji K, Pourfath M and Fathipour M 2013 J. Appl. Phys. 113 163708

- [5] Shidpour R and Manteghian M 2010 Nanoscale 2 1429
- [6] Ataca C and Ciraci S 2011 J. Phys. Chem. C 115 13303
- [7] Zhou Y, Yang P, Zu H, Gao F and Zu X 2013 Phys. Chem. Chem. Phys. 15 10385
- [8] Enyashin A, Bar-Sadan M, Houben L and Seifert G 2013 J. Phys. Chem. C 117 10842
- [9] He J, Wu K, Sa R, Li Q and Wei Y 2010 Appl. Phys. Lett. 96 082504
- [10] Huang Z, Hao G, He C, Yang H, Xue L, Qi X, Peng X and Zhong J 2013 J. Appl. Phys. 114 083706
- [11] Chen J, Kuriyama N, Yuan H, Takeshita H T and Sakai T 2001 J. Am. Chem. Soc. 123 11813
- [12] Mosleh M, Atnafu N, Belk J and Nobles O 2009 Wear 267 1220
- [13] Mak K, Lee C, Hone J, Shan J and Heinz T 2010 Phys. Rev. Lett. 105 136805
- [14] Kibsgaard J, Tuxen A, Knudsen K, Brorson M, Topsoe H, Laegsgaard E, Lauritsen J and Besenbacher F 2010 J. Catal. 272 195
- [15] Chang K and Chen W 2011 ACS Nano 5 4720
- [16] Radisavljevic B, Radenovic A, Brivio J, Giacometti V and Kis A 2011 Nat. Nanotechnol. 6 147
- [17] Lukashev P, Kidd T, Harms H, Gorgen C and Stollenwerk A 2024 Appl. Phys. Lett. 124 083103
- [18] Ma Y, Dai Y, Guo M, Niu C, Lu J and Huang B 2011 Phys. Chem. Chem. Phys. 13 15546
- [19] Wang Y, Wang B, Huang R, Gao B, Kong F and Zhang Q 2014 Physica E 63 276
- [20] Kidd T, Kruckenberg P, Gorgen C, Lukashev P and Stollenwerk A 2022 J. Appl. Phys. 132 245301
- [21] Zhou Y, Zu X, Gao F, Lv H and Xiao H 2009 Appl. Phys. Lett. **95** 123119
- [22] Sevinçli H, Topsakal M, Durgun E and Ciraci S 2008 Phys. Rev. B 77 195434
- [23] Gao D, Shi S, Tao K, Xia B and Xue D 2015 Nanoscale 7 4211
- [24] Singla R, Kumar S, Hackett T, Reshak A and Kashyap M 2021 J. Alloys Compd. 859 157776
- [25] Kidd T, Weber J, Holzapfel R, Doore K and Stollenwerk A 2018 Appl. Phys. Lett. 113 191603
- [26] Kidd T, O'Leary E, Anderson A, Scott S and Stollenwerk A 2019 Phys. Rev. B 100 235447
- [27] Kresse G and Joubert D 1999 Phys. Rev. B 59 1758
- [28] Blöchl P 1994 Phys. Rev. B 50 17953
- [29] Perdew J P, Burke K and Ernzerhof M 1996 *Phys. Rev. Lett.* 77 3865
- [30] Methfessel M and Paxton A T 1989 Phys. Rev. B 40 3616
- [31] MedeA-2.22 2017 (Materials Design Inc)
- [32] Towns J et al 2014 XSEDE: accelerating scientific discovery Comput. Sci. Eng. 16 62–74
- [33] Kidd T, Shand P, Stollenwerk A, Gorgen C, Moua Y, Stuelke L and Lukashev P 2022 AIP Adv. 12 035233
- [34] Harms H Cunningham C Kidd T and Stollenwerk A2024 Surface dependence of electronic growth of Cu(111) on MoS₂ Appl. Phys. Lett. 125 081604
- [35] Kidd T, Weber J, O'Leary E and Stollenwerk A 2021 Langmuir 37 9472
- [36] Lebègue S and Eriksson O 2009 Phys. Rev. B 79 115409
- [37] Saidi W 2015 Cryst. Growth Des. 15 3190
- [38] Agrachev M, Antonello S, Dainese T, Ruzzi M, Zoleo A, Aprà E, Govind N, Fortunelli A, Sementa L and Maran F 2017 ACS Omega 2 2607